Influence of Different Copolymer Sequences in Low Band Gap Polymers on Their Performance in Organic Solar Cells

Alexander Lange,[1] Hartmut Krueger,[1] Bernhard Ecker,[2] Ali Veysel Tunc,[2] Elizabeth von Hauff,[2] Mauro Morana[3]

[1]Fraunhofer Institute for Applied Polymer Research, Geiselbergstrasse 69, 14476 Potsdam-Golm, Germany
[2]Energy and Semiconductor Research Laboratory, Institute of Physics, Carl von Ossietzky University, 26111 Oldenburg, Germany
[3]Konarka Austria Forschungs und Enwicklungs GmbH, Altenbergerstr. 69, 4040 Linz, Austria
Correspondence to: H. Krueger (E-mail: krueger@iap.fhg.de)

ABSTRACT: The chemical design of a polymer can be tailored by a random or a block sequence of the comonomers in order to influence the properties of the final material. In this work, two sequences, PCPDTBT and F8BT (F8), were polymerized to form a block or a random copolymer. Differences between the various polymers were examined by exploring the surface topography and charge carrier mobility. A distinct surface texture and a higher charge carrier mobility was found for the block copolymer with respect to the other materials. Solar cells were prepared with polymer:$PC_{71}BM$ blend active layers and the best performance of up to 2% was found for the block copolymer, which was a direct result of the fill factor. Overall, the sequences of different copolymers for solar cell applications were varied and a positive impact on efficiency was found when the block copolymer structure was utilized. © 2012 Wiley Periodicals, Inc. J Polym Sci Part A: Polym Chem 50: 1622–1635, 2012

KEYWORDS: diblock copolymers; morphology; organic solar cells; phase behavior; random copolymers

INTRODUCTION Due to increasing energy demands around the world and the need for green energy resources, research activities in the field of organic photovoltaics (OPV) have steadily grown during the past 10 years.[1–3] The most successful type of OPV device utilizes a mixture of an electron donating and an electron accepting species in a bulk heterojunction. This device concept utilizes a large interfacial area between both components to facilitate the splitting of excitons into free charges at phase boundaries, providing proper energy level alignment between the electron donor and acceptor.[4] Electrons and holes are subsequently transported to the electrodes via pure phases of the respective components. Many studies have explored solar cells with the standard materials system, semicrystalline poly(3-hexylthiophene) (P3HT), and phenyl-C_{61}-butyric acid methyl ester ($PC_{61}BM$). Power conversion efficiencies (η_{PCE}) of up to 5% have been reported for devices based on P3HT:$PC_{61}BM$.[5] In addition to a large emphasis on P3HT:$PC_{61}BM$, the synthesis of novel materials has emerged and the focus has partially shifted to investigate polymers, such as poly[2,1,3-benzothiadiazole-4,7-diyl[4,4-bis(2-ethylhexyl)-4H-cyclopenta[2,1-b:3,4-b′]dithiophene-2,6-diyl]] (PCPDTBT), which have absorbance maximums at longer wavelengths with respect to P3HT. The main goal of using low band gap materials is to harvest as much light as possible from the sun's spectrum in order to increase device performance.[6–10] In comparison to P3HT, which absorbs only 46% of the incident light from the sun, PCPDTBT absorbs close to 64%[11] Due to its good solubility and good matching of fullerene's electronic levels, PCPDTBT is an interesting candidate for high-efficiency solar cells. However, an unfavorable, highly intermixed nanomorphology observed in as-cast blends with PCBM seems to reduce the possible applications of this polymer.[6] Therefore, other low band gap polymers have been synthesized and developed and device efficiencies of over 7% have been reported which demonstrates the potential of novel materials for solar cells.[12]

As previously reported, thermal annealing has a major impact on the properties of P3HT:$PC_{61}BM$ thin films where a correlation between the treatment temperature and degree of crystallinity was found.[13] Correspondingly, thermal treatments were shown to directly impact the performance of P3HT:$PC_{61}BM$ solar cells as well as their stability.[5,14,15] In addition, the degree of organization in P3HT:$PC_{61}BM$ films can be influenced with non-thermal treatments such as solvent annealing where films are allowed to dry for an extended period of time after spin coating in a solvent-saturated atmosphere.[15] Nonetheless, the degree of organization

Additional Supporting Information may be found in the online version of this article.

in P3HT:PC$_{61}$BM films is an important aspect when preparing high performance devices. In contrast to P3HT, the properties, such as absorbance, of PCPDTBT do not improve upon annealing.[12] Other methods are then employed to induce morphology changes in PCPDTBT films such as processing with solvent additives, i.e., diiodo-octane (DIO) or octane dithiol (ODT).[7,16,17] Different requirements must be fulfilled when using an additive in order to achieve good results. First, the additive should have a higher boiling point than the common solvent.[18] Second, only the fullerene species and not the polymer should be soluble in the additive.[17] Due to the boiling point and solubility properties of the additive, the polymer precipitates prior to the fullerene species from the common solution during processing. Correspondingly, the polymer can phase separate from the fullerene, forming an enhanced network which can lead to better device performance. When comparing the three major ways to influence the morphology of polymer–fullerene thin films, the use of solvent additives was shown to be the most useful for low band gap materials.[6,19] The use of additives may however complicate solution processing and does not always offer a favorable way to coat polymer–fullerene blends with roll-to-roll methods.

Electron accepting polymers such as poly(9,9-dioctylfluorene-*alt*-benzothiadiazole) (F8BT) can be used to create polymer–polymer donor–acceptor systems. F8BT's highest occupied molecular orbital (HOMO) and lowest unoccupied molecular orbital (LUMO) levels are well positioned with those of P3HT in addition to poly(vinyl carbazole) (PVK) for efficient charge transfer as studies on blends of P3HT:F8BT and PVK:F8BT have shown.[20,21] For the PVK:F8BT devices, the weight ratio of PVK to F8BT was found to directly impact performance and the surface topography of the device active layer.[21] However, polymer–polymer solar cells typically suffer from low short circuit current densities (J_{sc}) when compared to devices with PC$_{61}$BM.[22] Despite the low performance of polymer–polymer devices with respect to solar cells based on polymers mixed with PC$_{61}$BM or PC$_{71}$BM, the chemical properties of F8BT can be exploited for solar cell applications. Specifically, the electron donating and electron accepting potentials of different monomers which are combined and polymerized have a direct impact on the properties of the resulting polymer.[23] This concept has been explored in the literature for polymers with different donor–acceptor (DA) or donor–acceptor donor (DAD) units for solar cell applications where the band gap was found to vary with the strength of the electron accepting unit.[23]

In this work, we synthesized three amorphous, low band gap polymers and used a solvent additive (DIO) to process thin films for organic solar cells. In preparing fullerene blend films, we used DIO as a solvent additive instead of ODT because it was found to improve film quality. In addition, other works have reported similar or even better device efficiencies for films prepared with DIO as compared to ODT.[17] The polymer species examined here are pure PCPDTBT, a block copolymer of PCPDTBT with F8 (PCPDTBT-*block*-F8) and a random copolymer of PCPDTBT with F8BT (PCPDTBT-*co*-F8BT). In order to determine the impact of the chemical
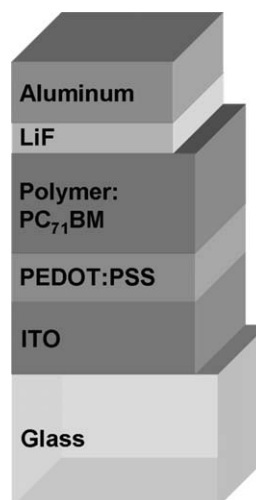
FIGURE 1 The solar cell structure used in this report.

structure of the electron donating species on solar cell performance, active layers were prepared with blends of the previously mentioned polymers with PC$_{71}$BM. For better understanding and characterizing the impact of the copolymers on performance, ternary blends of PCPDTBT, F8BT and PC$_{71}$BM were also examined in solar cells with the device structure shown in Figure 1. Here, we analyze the impact of different copolymer sequences on device performance and surface topography. The novel PCPDTBT-*block*-F8 shows the best solar cell performance of all the blends investigated.

RESULTS AND DISCUSSION

Chemistry

For synthesizing the PCPDTBT homopolymer, random PCPDTBT-*co*-F8BT copolymer and PCPDTBT-*block*-F8 copolymer new synthesis procedures were developed. The PCPDTBT homopolymer and the random PCPDTBT-*co*-F8BT copolymer were polymerized via Suzuki-coupling. PCPDTBT-*block*-F8 was polymerized in two steps and a polymer analogous reaction. All polymers were analyzed with differential scanning calorimetry to examine their thermal behavior. For all polymers no thermal transitions and no degradation effects were found up to 250 °C. Glass transitions could not be determined using this method. In the following, a detailed description will be given.

Monomers

The 2,6-bis(4,4,5,5-tetramethyl)-[1,3,2]dioxaborolane-4,4-bis (2-ethylhexyl)-4H-cyclopenta-[2,1-b:3,4-b′]dithiophene monomer was synthesized following an eight-step procedure. The first six steps were in accordance with literature.[24] The seventh and eighth steps were in accordance with general organic reactions of bromination and boronic ester synthesis.

The 5,8-dibromo-2,1,3-benzothiadiazole was obtained by bromination of 2,1,3-benzothiadiazole using bromine in hydrobromic acid.

PCPDTBT Homopolymer

For the PCPDTBT homopolymer, a Stille coupling procedure is typically applied in the literature.[24] Pisula et al. used

TABLE 1 Overview of the Number Average (M_n) and Weight Average (M_w) Molecular Weights, Polydispersity Indexes (PDI) and Compositions of the Polymers Synthesized in this Work

	Molar ratio		10^3 g/mole		
Polymer	PCPDTBT	F8BT (or F8)	M_n	M_w	PDI
PCPDTBT	1	0	11.7	31.0	2.65
PCPDTBT-co-F8BT	0.66	0.34	9.0	22.5	2.5
PCPDTBT-block-F8	0.94	0.06	17.8	34.3	1.93
F8BT	0	1	3.7	8.4	2.27

Suzuki coupling as the polymerization technique.[25] They used diboronic ester of 5,8-dibromo-2,1,3-benzothiadiazole and 2,6-dibromo-4,4-bis(2-ethylhexyl)-4H-cyclopenta[2,1-b:3,4-b′]dithiophene as monomers. We used a modified Suzuki coupling (Fig. 2) for this step by changing the dibromo and the diboronic ester monomers. Therefore, we introduced a novel dicyclohexylphosphino-2′,6′-dimethoxybiphenyl (dhpdb) ligand for the Pd(II) acetate catalyst. Satisfying molecular weights were obtained only with this ligand after treatment under reflux conditions (Table 1). Nevertheless, the M_n of our Suzuki-coupled PCPDTBT is still somewhat lower than what is obtained for the Stille-coupling polymerization.

Random PCPDTBT-co-F8BT

The synthesis of the PCPDTBT-co-F8BT was carried out by Suzuki copolymerization using equimolar moles of 2,6-bis(4,4,5,5-tetramethyl)-[1,3,2]dioxaborolane-4,4-bis(2-ethyl-hexyl)-4H-cyclopenta[2,1-b:3,4-b′]dithiophene and 2,7-bis (4,4,5,5-tetramethyl-[1,3,2]dioxaborolane)-9,9-dioctylfluorene (Fig. 3, with $n = m$). An enrichment of the dithiophene monomer in the copolymer (0.66–0.34 molar ratio) was found. The molecular weights were in the same range as for the PCPDTBT homopolymer.

PCPDTBT-block-F8

The block-copolymer synthesis was carried out in a two-step procedure (Fig. 4). First, a Yamamoto polymerization was chosen to generate the F8-block. The polymerization was done in the presence of a 2-bromo-thiophene end-capping agent. By adjusting the molar ratio of dibromo-F8 and 2-bromo-thiophene, the molecular weight can be controlled.

The obtained thiophene-terminated F8-block was brominated in the five-position of the thiophene end groups using NBS in a polymer analogous reaction. The experimental molecular

weights of the thiophene- and the 5-bromothiophene-terminated F8-blocks are shown in Table 2.

The thiophene end groups were identified by the corresponding NMR signals at 7.40, 7.30, and 7.12 ppm for the three protons of the thiophene. The success of thiophene end group bromination was also determined with ^{1}H NMR by the two remaining signals at 7.13 and 7.06 ppm. By comparing the molecular weights (Table 2), it can be seen that no significant change took place during bromination; thus, degradation can be excluded.

The obtained 5-bromothiophene-terminated F8-block was introduced in the second step Suzuki-polymerization. Therefore, the 2,6-bis(4,4,5,5-tetramethyl)-[1,3,2]dioxaborolane-4,4-bis(2-ethylhexyl)-4H-cyclopenta[2,1-b:3,4-b′]dithiophene ($n + z$) was used as a diboronic acid comonomer in a 24/1 molar ratio to the 5-bromothiophene-terminated F8-block ($z = 1$) with an equimolar amount of 5,8-dibromo-2,1,3-benzothiadiazole ($n = 23$) (Fig. 5).

The obtained PCPDTBT-block-F8 shows comparable molecular weights as the homopolymer PCPDTBT. Because of the chosen molar monomer ratio, the PCPDTBT-block is found to exceed 94 mole% in the block copolymer during polymerization.

Energy Levels of the Polymers

The energy levels of the different polymers were estimated by cyclovoltammetric measurements in films on glassy carbon electrodes. The results are summarized in Table 3.

In the PCPDTBT-containing polymers, the HOMO- and the LUMO-levels were determined by the PCPDTBT-sequence, resulting in similar values. The block-copolymer exhibits exactly the same levels as the homopolymer. The random copolymer shows just a little wider electrochemical band gap which agrees with the lower absorption maximum compared to the homo- and the block-copolymers. Finally, F8BT has a significantly wider band gap with a considerably lower HOMO level and a slightly higher LUMO level. The HOMO levels of the different polymers in Table 3 align well with the work function of poly(3,4-ethylenedioxythiophene): poly (styrenesulfonate) (PEDOT:PSS) (∼5 eV) which eliminates potential hole extraction barriers.[21] In addition, the energy difference between the LUMO levels of the polymers and PC$_{71}$BM is large enough (0.9–1.0 eV) to effectively split excitons. Values for PC$_{71}$BM were taken from ref. 23 which found values of −4.1 eV and −6.5 eV for the HOMO and LUMO, respectively. Overall, the energy levels of PCPDTBT,
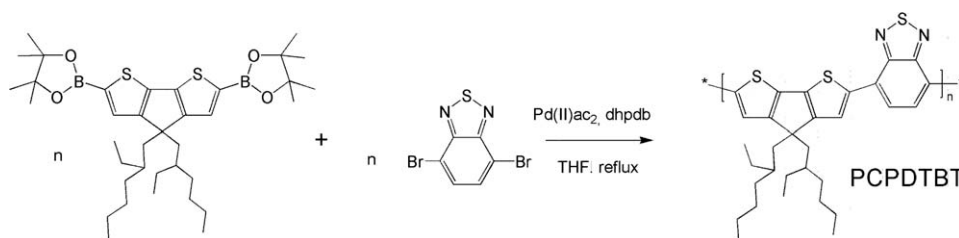
FIGURE 2 Synthesis of PCPDTBT homopolymer by SUZUKI-coupling.
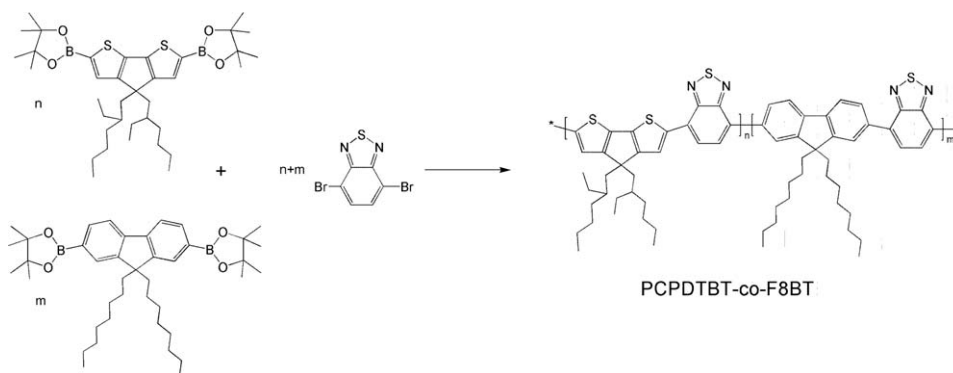
FIGURE 3 Synthesis of random PCPDTBT-*co*-F8BT by SUZUKI-coupling.

PCPDTBT-*co*-F8BT, and PCPDTBT-*block*-F8 are well suited for solar cell applications.

Optical Properties of the Pure Polymers and Polymer: $PC_{71}BM$ Films

The absorption behavior of the different polymers with comparable film thicknesses are summarized in Figure 6. F8BT shows the expected spectrum with two maxima at 331 and 465 nm.[26] The optical band gap of PCPDTBT is shifted to longer wavelengths with respect to F8BT where the absorbance maximum and edge are found at 730 and 900 nm, respectively. The measured peaks for pure PCPDTBT agree well with reports in literature.[27] For the random PCPDTBT-*co*-F8BT copolymer, absorbance ends already at 810 nm and the maximum is shifted to 664 nm. The considerable blue shift for this material can be explained by random arrangement of the PCPDTBT and F8BT sequences. More specifically, the PCPDTBT sequences are diluted with the F8BT sequences and the resulting conjugation length is shorter with respect to the homopolymer. In case of the block copolymer, nearly the same peaks are found as for the PCPDTBT homopolymer. However, the appearance of a weak shoulder in the spectrum of PCPDTBT-*block*-F8 indicates an enhanced organization within the thin film which corresponds well to the AFM analysis which will be discussed in detail later. Shoulders in the absorbance spectra of PCPDTBT have been found upon processing with additives which resulted in more organized films.[28] In general, a decrease in the low band gap absorbance was found with increasing F8-content in the polymers examined here.

In order to understand the optical properties of thin films consisting of the different polymers blended with $PC_{71}BM$,

UV-Vis spectroscopy was used as shown in Figure 7. When the spectra of the pure polymers shown in Figure 6 are compared to those of the blends presented in Figure 7(a), the peak from the polymer absorbance at longer wavelength is seen in addition to the broad absorbance of $PC_{71}BM$ within the visible region. The intensities of the peaks around a 750-nm mirror those of the pure polymers where PCPDTBT-*block*-F8 has the highest intensity followed by PCPDTBT and PCPDTBT-*co*-F8BT. However, the intensities of the peaks are also influenced by small layer thickness differences. A close-up of the absorption spectra between 575 and 900 nm is shown in Figure 7(b). Interestingly, no distinct peak is seen at longer wavelengths for PCPDTBT-*co*-F8BT:$PC_{71}BM$. Instead, the spectrum from $PC_{71}BM$ overlaps with the peak from the polymer because of its considerable blue shift with respect to the other polymers. Upon addition of F8BT to PCPDTBT (1:1), a peak at 462 nm becomes visible, which corresponds to the absorbance of pure F8BT. For a homopolymer blend of PCPDTBT:F8BT with less F8BT (1:0.5), the peak for F8BT overlaps with the spectrum of $PC_{71}BM$.

Photoluminescence

Photoluminescence (PL) measurements are an important characterization method for electron donor and acceptor films. Ideally, the majority of the photoluminescence from an electron donor should be fully quenched upon addition of an electron acceptor like $PC_{71}BM$, due to the charge transfer from donor to acceptor sites. PL measurements were performed on PCPDTBT, PCPDTBT-*block*-F8, and PCPDTBT-*co*-F8BT with and without $PC_{71}BM$ as shown in Figure 8(a,b). Excitation wavelengths of 420 and 550 nm were used for Figure 8(a,b), respectively.

thiophene-terminated F8-block

5-bromothiophene-terminated F8-block
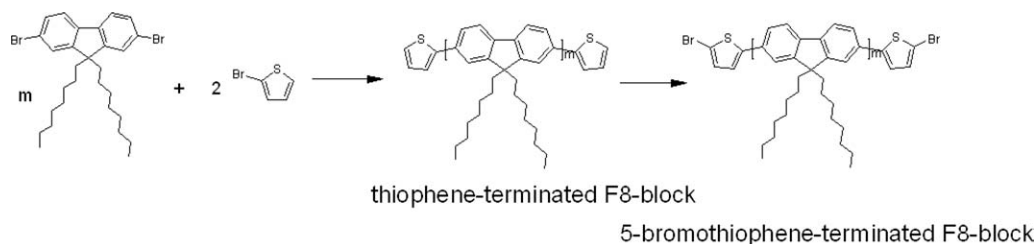
FIGURE 4 Synthesis of 5-bromothiophene-terminated F8-block for block copolymer approach.

TABLE 2 Experimental Molecular Weights of the Thiophene- and the 5-Bromothiophene-Terminated F8-Blocks

	g/mole			
	Found[a]	M_n[b]	M_w[b]	PDI
Thiophene-terminated F8-block	2265	1137	2896	2.55
5-bromothiophene-terminated F8-block	2422	1386	2636	1.90

[a] Calculated from elemental analysis, S-content.
[b] Obtained by GPC using polystyrene calibration.

Upon excitation at 550 nm, PL maxima between 790 and 800 nm were found for PCPDTBT, PCPDTBT-block-F8, and PCPDTBT-co-F8BT [Fig. 8(b)]. As expected, the PL maxima are red shifted with respect to the absorbance maxima for the pure polymers. For the polymer blends with $PC_{71}BM$, the PL maxima between 790 and 800 nm are almost completely quenched. The insert in Figure 8(b) shows minor differences between the three blends, all showing a quenching ratio of over two orders of magnitude at the polymer maximum emission, indicating rather efficient exciton collection and charge transfer. From other works, the maximum PL intensity for PCPDTBT was reported between 872 and ~950 nm.[6,11,29–31] Additionally, the PCPDTBT absorbance maximum was measured between 730 and ~775 nm.[6,11,29,30] We propose that the lower values for the absorbance and PL peaks for our polymers could be related to their relatively low molecular weights as compared to other works.[6,11]

As seen in the absorbance spectra of the pure polymers, an additional maximum at shorter wavelengths around ~400 nm was also found. Upon excitation of the pure polymer films with 420 nm, a second PL maximum for each polymer was found in Figure 8(a). To our knowledge, this PL peak has not been examined in detail in the literature. In this situation, the PL peaks at 420 nm are not completely quenched upon addition of $PC_{71}BM$. The exact cause of this additional PL peak at shorter wavelengths is unclear. Different processes occur upon exciting the pure polymers or the blends at 420 nm. For the pure polymers, the F8BT units are most likely excited and fluoresce. However, a similar trend is also seen for PCPDTBT where no F8BT is present. In the blend systems, both the F8BT units from the different polymers

absorb light in addition to $PC_{71}BM$ (Fig. 7, UV-Vis from blends). Therefore, a direct comparison of the blend and pure polymer PL spectra upon excitation at 420 nm is difficult.

Solar Cell Characteristics

In order to describe the influence of the different polymer structures on the charge mobilities in the polymer films, OFETs were fabricated in a bottom-gate structure. From the current-voltage characteristics, hole mobilities were calculated. They are summarized in Table 3. It can be clearly seen that for the polymers with larger PCPDTBT sequences (PCPDTBT homo- and block copolymer), a hole mobility in the range of 10^{-3} cm^2/Vs was found. In contrast, the random copolymer (PCPDTBT-co-F8BT) exhibits a hole mobility of one order of magnitude lower. Additionally, the block copolymer shows a hole mobility two times higher than the PCPDTBT homopolymer which should result in a better charge transport ability in solar cells with the block copolymer/$PC_{71}BM$-blend films.

Solar cells were prepared with the different polymers combined with $PC_{71}BM$ and measured under illumination as shown in Figure 9(a). Dark current-voltage characteristics are shown in the Supporting Information. The devices were further characterized with external quantum efficiency (EQE) measurements. A summary of the data from Figure 9(a,b) is given in Table 4.

As shown in Figure 9(a) and Table 4, devices with PCPDTBT-block-F8 had the highest η_{PCE} values of ~2.0% followed by PCPDTBT and PCPDTBT-co-F8BT. This result corresponds well to the UV-Vis spectra for the block-copolymer and the higher OFET mobility with respect to the other polymers. Low efficiencies for PCPDTBT-co-F8BT can partially be explained by the small amount of light which this polymer absorbs at longer wavelengths in addition to the reduced hole mobility. The lower light absorption for the random copolymer at longer wavelengths is a result of the random distribution of the copolymer sequences. The absorbance spectrum showed that the majority of light which this system absorbs is due to $PC_{71}BM$ and not the polymer. Interestingly, slightly larger V_{oc} values were found for devices with PCPDTBT-co-F8BT which is related to the polymer's relatively high HOMO level. This result corresponds to previously reported results where the V_{oc} of organic solar cells is
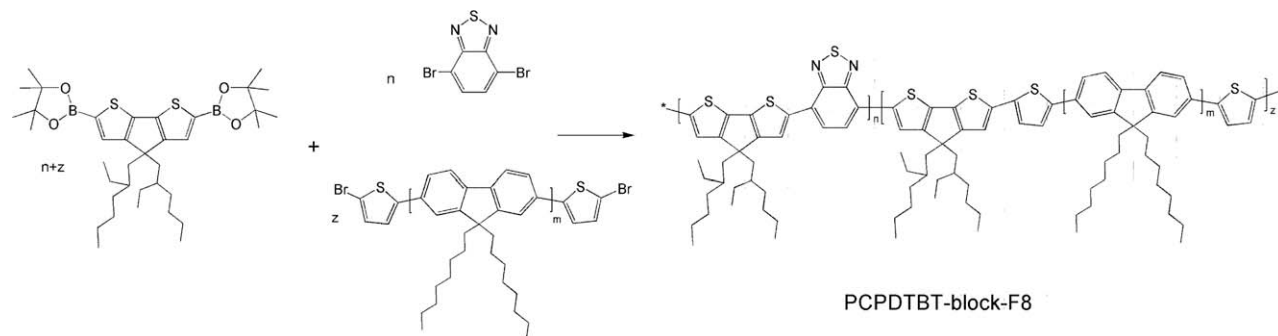
FIGURE 5 Synthesis of PCPDTBT-block-F8.

TABLE 3 Estimated Energy Levels from CV and Calculated OFET Hole Mobilities of the Synthesized Polymers

	Molar ratio		eV			10^{-3} cm^2/Vs
Polymer	PCPDTBT	F8BT (or F8)	HOMO	LUMO	Band Gap (CV)	μ_{hole}
PCPDTBT	1	0	−5.1	−3.2	1.9	1.4
PCPDTBT-*co*-F8BT	0.66	0.34	−5.2	−3.1	2.1	0.11
PCPDTBT-*block*-F8	0.94	0.06	−5.1	−3.2	1.9	2.3
F8BT	0	1	−5.9	−3.0	2.9	0.1

directly related to the HOMO and LUMO levels of the donor and acceptor, respectively.[23]

In order to better understand how the chemical composition of the electron-donating polymer species impacts device performance, solar cells were prepared with ternary blends of PCPDTBT, F8BT, and PC$_{71}$BM. Upon addition of F8BT to PCPDTBT, device performance decreased as shown in Table 4 where considerably smaller J_{sc} and FF values were found. As shown in the absorbance spectra in Figure 7(b), a distinct blue shift is seen for the PCPDTBT:F8BT blend ratio of 1:1 which indicates a more unorganized system with respect to the 1:0.5 PCPDTBT:F8BT system. Overall, both ternary blends are blue shifted with respect to PCPDTBT:PC$_{71}$BM. Overall, combination of two homopolymers, F8BT and PCPDTBT, results in reduced solar cell performance.

From the EQE data in Figure 9(b), the sensitivity of the devices at wavelengths greater than 700 nm in comparison to a traditional P3HT:PC$_{61}$BM solar cell is demonstrated. The highest EQE was observed for PCPDTBT-*block*-F8 followed by PCPDTBT and PCPDTBT-*co*-F8BT which mirrors the J_{sc} values in Table 4. For comparison purposes, a device was prepared with F8BT:PC$_{71}$BM. Despite the necessary HOMO and LUMO level offset between F8BT and PC$_{71}$BM (Table 3), small EQE values were measured which may be a result hindered hole transport. Thus, the enhanced EQE of PCPDTBT-*block*-F8 is a result of the novel copolymer structure consisting of both PCPDTBT and F8 blocks.

A summary of the performance of the different blends for the systems examined in this report is shown in Figure 10. The best performance was found for the block copolymer consisting of PCPDTBT and F8 units. It is clearly seen that the ternary blends perform worse than the copolymers.

In comparison to what has been reported in the literature for solar cells with PCPDTBT:PC$_{71}$BM, the η_{PCE} values for our devices are lower. It has been reported that η_{PCE} values of between 3 and 6% are achievable for PCPDTBT:PC$_{71}$BM when processed from chlorobenzene with additives.[6,7] The
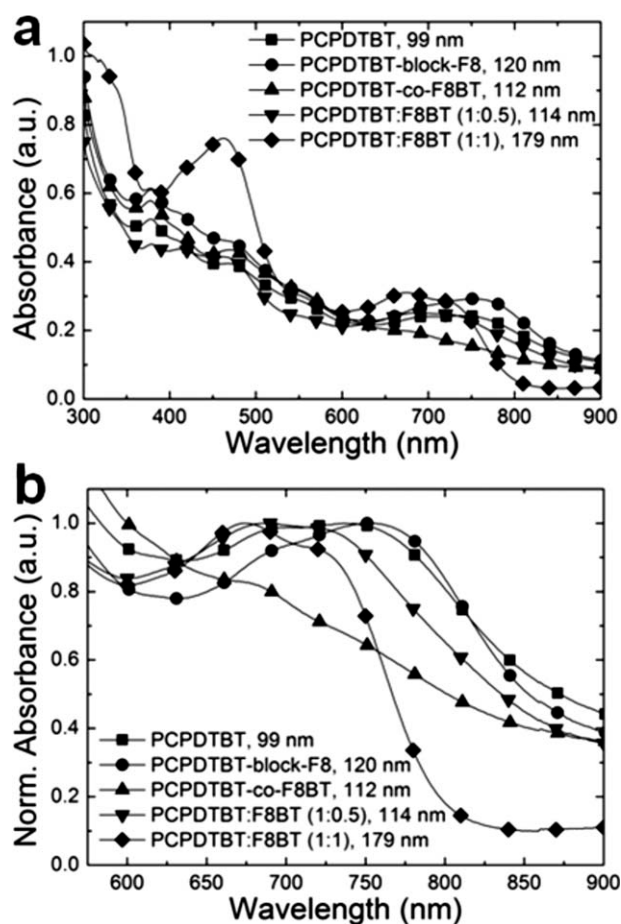
FIGURE 7 Absolute absorbance versus wavelength for PCPDTBT, PCPDTBT-*block*-F8, PCPDTBT-*co*-F8BT and PCPDTBT:F8BT blended with PC$_{71}$BM (a) and normalized absorbance between 575 and 900 nm (b). Please note that the ratio of the polymers to PC$_{71}$BM was 1:3 unless otherwise stated.

FIGURE 6 Absolute absorbance versus wavelength for PCPDTBT, PCPDTBT-*block*-F8, PCPDTBT-*co*-F8BT and F8BT.

ARTICLE
WWW.POLYMERCHEMISTRY.ORG

JOURNAL OF
POLYMER SCIENCE
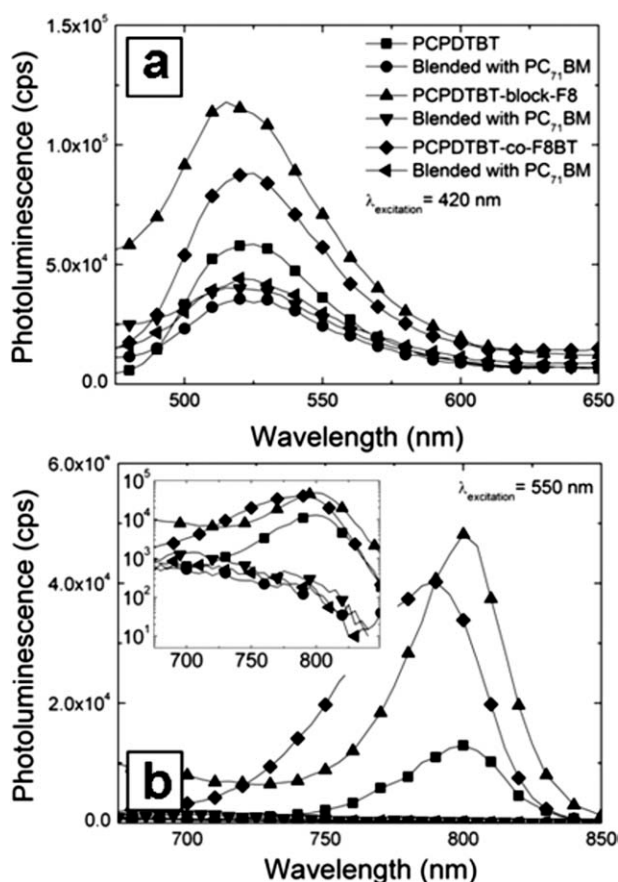
Polymer
Chemistry

FIGURE 8 Photoluminescence versus wavelength for pure PCPDTBT, PCPDTBT-*block*-F8 and PCPDTBT-*co*-F8BT and for the polymers blended with $PC_{71}BM$ upon excitation at 420 nm (a) or 550 nm (b). The insert in (b) shows the quenching data on a semilog scale for comparison purposes.

cause of the lower performance for our PCPDTBT which was obtained via SUZUKI-polymerization is mainly related to the molecular weight. Commercially available PCPDTBT from 1-Material with a M_n of 19,900 g/mole resulted in solar cells with an increased J_{sc} (9 mA/cm^2) and FF (>50%). This trend agrees with other works which showed that the J_{sc} of PCPDTBT:$PC_{71}BM$ solar cells increases with M_n.[27]

AFM

Examination of the surface topography of thin films used for solar cells is useful because it can give insight into phase separation and device performance as previously shown.[15,17,20,21,32–35] To begin, films from pure PCPDTBT, PCPDTBT-*block*-F8, PCPDTBT-*co*-F8BT, and F8BT without $PC_{71}BM$ were examined with AFM as shown in Figure 11.

A distinct topography was found for PCPDTBT-*block*-F8 [Fig. 11(b)] in comparison to a smooth texture for PCPDTBT-*co*-F8BT [Fig. 11(c)]. The surface topography of PCPDTBT [Fig. 11(a)] was more distinct than that of PCPDTBT-*co*-F8BT but not as apparent as for PCPDTBT-*block*-F8. The different surface topographies are partially reflected in root mean square
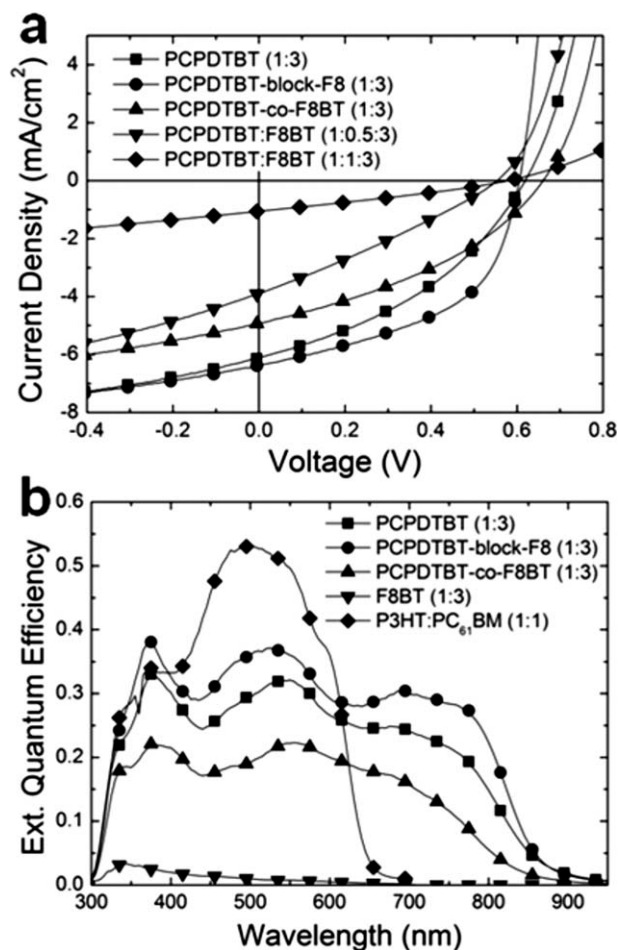
FIGURE 9 Current density versus voltage for devices with PCDTBT, PCPDTBT-*block*-F8, PCPDTBT-*co*-F8BT, or PCPDTBT+F8BT blended with $PC_{71}BM$ (a) and external quantum efficiency versus wavelength for devices with PCDTBT, PCPDTBT-*block*-F8, PCPDTBT-*co*-F8BT, or F8BT blended with $PC_{71}BM$ (1:3) (b). A P3HT:$PC_{61}BM$ device is shown in (b) for comparison purposes.

roughness (R_{rms}) values for the different films, where 0.7, 0.9, 0.5, and 0.7 nm were found for PCPDTBT, PCPDTBT-*block*-F8, PCPDTBT-*co*-F8BT, and F8BT, respectively. However, the differences in the surface profiles of the different polymers are most apparent upon visual inspection of the images in Figure 11 and not by direct comparison of the roughness

TABLE 4 Solar Cell Performance Summary for Devices with Different Polymer:$PC_{71}BM$ Active Layers

Polymer(s)	Thickness (nm)	V_{oc} (V)	J_{sc} (mA/cm^2)	FF (%)	η_{PCE} (%)
PCPDTBT	116	0.620	6.14	38.0	1.45
PCPDTBT-*block*-F8	112	0.610	6.38	49.9	1.94
PCPDTBT-*co*-F8BT	120	0.665	4.94	36.8	1.21
PCPDTBT:F8BT (1:0.5)	114	0.555	3.91	28.3	0.61
PCPDTBT:F8BT (1:1)	179	0.580	1.06	28.8	0.18
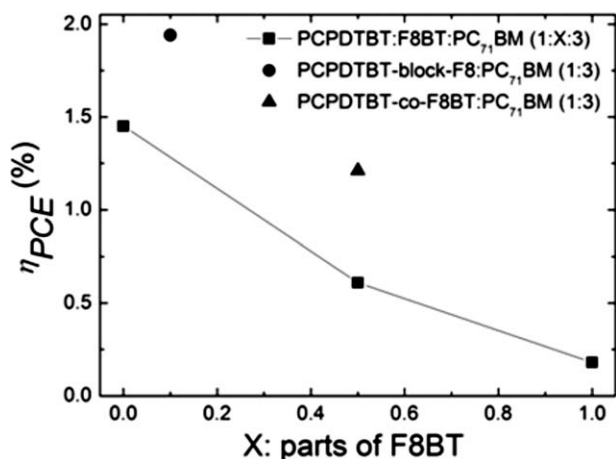
FIGURE 10 η_{PCE} as a function of the amount of F8BT in solar cells with active layers based on PCPDTBT:F8BT:PC$_{71}$BM (1:X:3) in comparison to devices with PCPDTBT-block-F8:PC$_{71}$BM (1:3) (circles) or PCPDTBT-co-F8BT:PC$_{71}$BM (1:3) (triangles) active layers.

values. The trend in the surface topographies is also mirrored in the phase contrast images where the largest and most distinct contrast was seen for PCPDTBT-block-F8 [Fig. 11(f)]. Interestingly, both of the homo polymers used in this work (PCPDTBT and F8BT) have distinct surface features in both the topography and phase contrast images [Fig. 11 a,d,e,h)]. However, this is not the case for random copolymer where smooth and featureless images were generated. This suggests that a block copolymer structure based on PCPDTBT and F8 units results in phase separation which can be seen on a 2.5-μm scale. The regions of F8 or PCPDTBT in

the block copolymer are able to pack together and form distinct groups. This is not the case for the random copolymer where sequences of PCPDTBT are diluted with F8BT and vice versa.

AFM was also preformed on polymer blends with PC$_{71}$BM as shown in Figure 12. The topography images of the blends in Figure 12 show smooth and similar surface features for PCPDTBT, PCPDTBT-block-F8, PCPDTBT-co-F8BT, and PCPDTBT:F8BT (1:1) as seen in Figure 12(a–c,e). R_{rms} values of 0.5, 0.5, 0.3, and 0.7 nm were calculated, respectively. The topography was much rougher for PCPDTBT:F8BT (1:0.5) despite similar preparation conditions for all solutions where R_{rms} was 8.6 nm. Upon further addition of F8BT to PCPDTBT, a smooth topography was found with an R_{rms} of 0.7 nm. The exact cause of the rough topography for PCPDTBT:F8BT (1:0.5) is unclear. The phase contrast images show a more distinct phase signal for PCPDTBT, PCPDTBT-block-F8, and PCPDTBT:F8BT (1:1) [Figs. 12(f,g,j), respectively]. For PCPDBT:F8BT (1:0.5), the distinct phase contrast features are seen which is due to the rough film topography in Figure 12(d). In correlation with the images from the pure polymer films, the phase contrast image for PCPDTBT-co-F8BT:PC$_{71}$BM (1:3) shows little phase information. Again, the chemical nature of the two different copolymers has a direct impact on the thin film topography. Overall, the trends in the AFM images agree well with the other experimental results. Distinct phases are found for the block copolymer which also shows a red-shifted absorbance maximum (Fig. 6). The enhanced organization in this material also results in the highest OFET mobility and the highest η_{PCE} value which is mainly a result of the enhanced fill factor for the materials under consideration. In contrast, the random sequence in
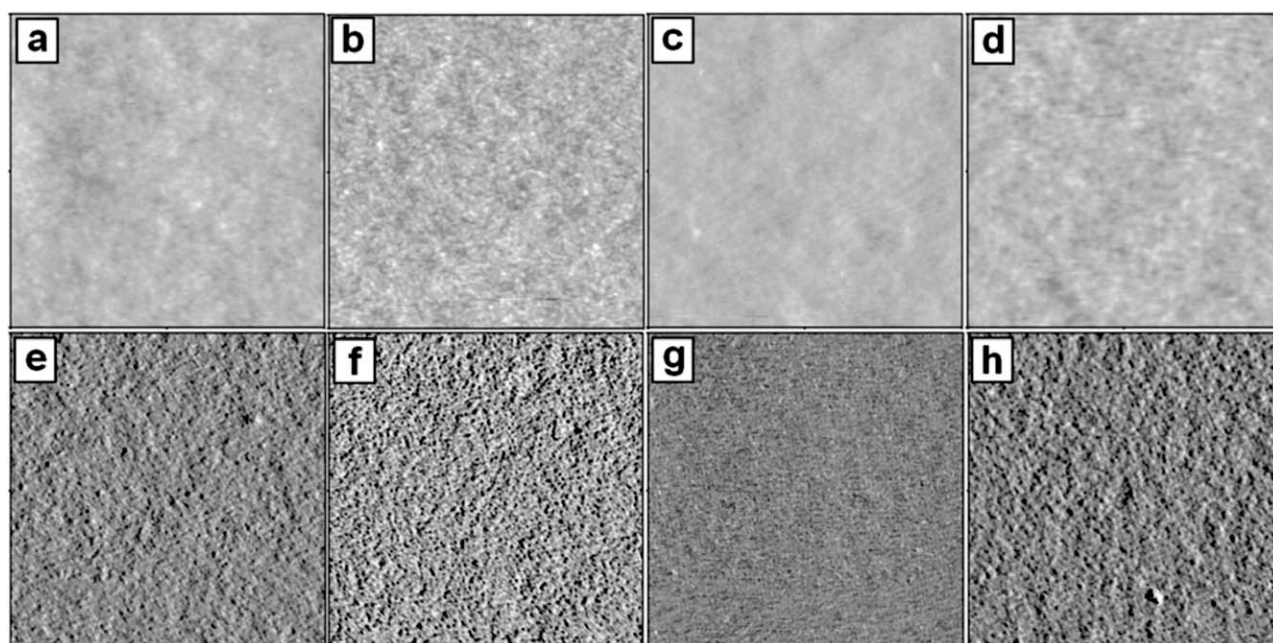
FIGURE 11 , AFM images of spin-coated PCPDTBT (a,e), PCPDTBT-block-F8 (b,f), PCPDTBT-co-F8BT (c,g) and F8BT (d,e) where a, b, c, and d are topography images (10.8 nm scale) and e, f, g, and h show phase contrast (2° scale).

ARTICLE

WWW.POLYMERCHEMISTRY.ORG

JOURNAL OF
POLYMER SCIENCE

Polymer
Chemistry
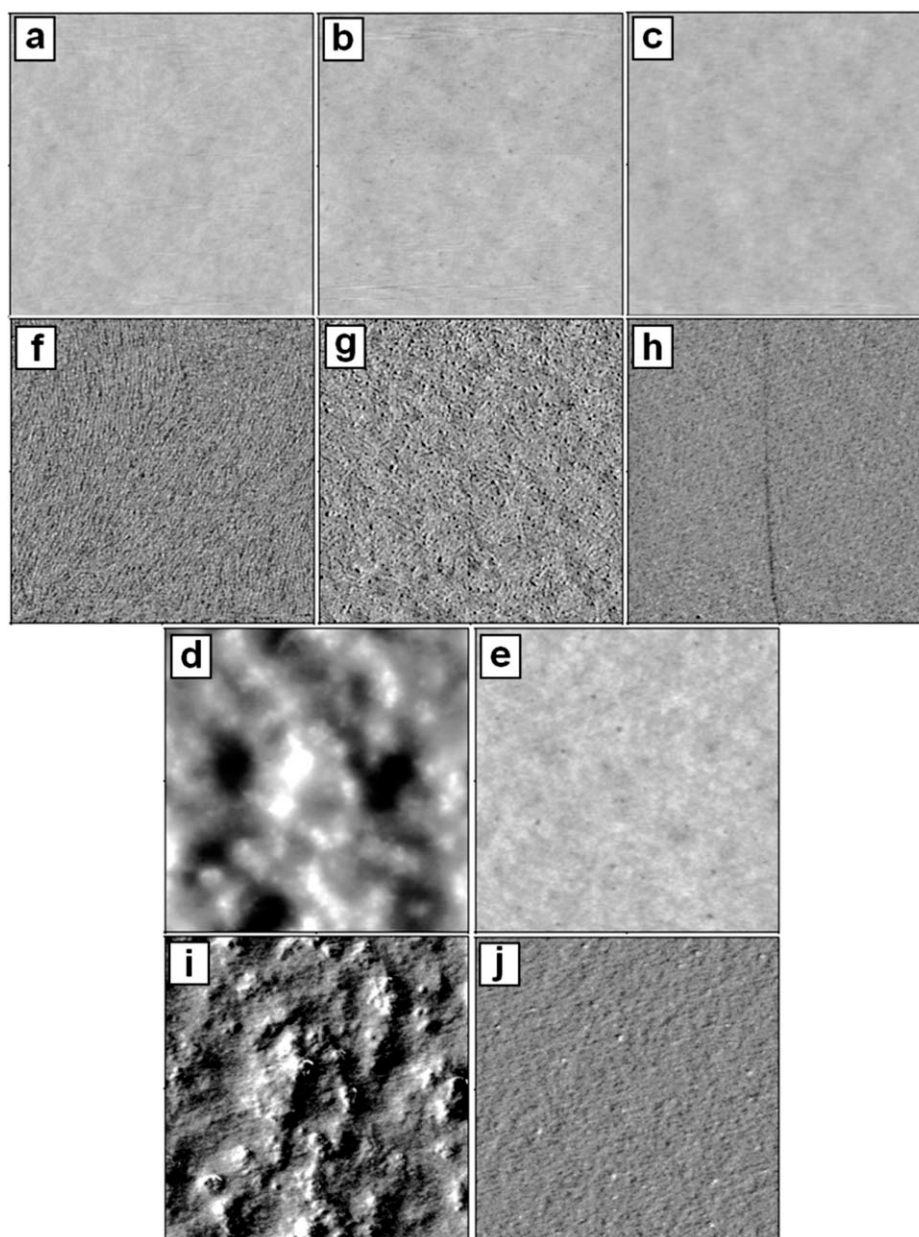
FIGURE 12 AFM images of spin-coated blends of PCPDTBT (a,f), PCPDTBT-*block*-F8 (b,g), PCPDTBT-*co*-F8BT (c,h), PCPDTBT:F8BT (1:0.5) (d,i), and PCPDTBT:F8BT (1:1) (e,j) all combined with three parts of $PC_{71}BM$, where a, b, c, d, and e are topography images (10.8 nm scale, except for i which has a 40-nm scale) and f, g, h, i, and j show phase contrast (2° scale).

PCPDTBT-*co*-F8BT results in a blue-shifted absorbance maximum (Fig. 6) which directly impacted J_{sc}. The mobility of the random copolymer was considerably lower than that of the block copolymer which corresponds to the feature-less surface topography seen in Figures 11 and 12. The trend seen here corresponds well to what has been found in the literature where rougher surface topographies which were determined with AFM resulted in devices with higher efficiencies.[33–35]

Upon comparison of the surface topographies of the blend and pure polymer films for PCPDTBT and PCPDTBT-*block*-

F8, distinct features are seen for the pure films, whereas feature-less surfaces were found for the blend films. In the block copolymer case, due to the difference between the surface energies of the two blocks and the fullerene, it is possible that some vertical phase separation between the block copolymer occurs at the PEDOT:PSS interface, as well as the formation of a vertical fullerene compositional gradient.

Vertical phase separation has been documented in P3HT:PC_{61}BM films where the surface energies of both blend components and the substrate play an important role.[36] The

surface roughness change for PCPDTBT and PCPDTBT-*block*-F8 may indeed suggest a different material composition at the film/air interface, which could consist of $PC_{71}BM$ or polymer:$PC_{71}BM$.

EXPERIMENTAL

Synthesis

All chemicals, reagents, and solvents were purchased from Sigma–Aldrich and Acros and were used as received unless further purification steps are described in this section. 2,7-Bis(4,4,5,5-tetramethyl-[1,3,2]dioxaborolane)-9,9-dioctylfluorene was used after twofold recrystallization from hexane.

Monomer Synthesis

2,6-Bis(4,4,5,5-tetramethyl)-[1,3,2]dioxaborolane-4,4-bis(2-ethylhexyl)-4H-cyclopenta[2,1-b:3,4-b′]dithiophene. The synthesis of 2,6-bis(4,4,5,5-tetramethyl)-[1,3,2]dioxaborolane-4,4-bis(2-ethylhexyl)-4H-cyclopenta[2,1-b:3,4-b′]dithiophen was mostly in accordance with literature procedures carried out in eight steps.[24]

2-Hydroxy-1,2-dithiophene-3-yl-ethanon

An argon-flooded reaction vessel was charged with 50 g (445.8 mmol) of thiophene-3-carbaldehyde, 5.96 g (22.1 mmol) of 3-benzyl-5-(2-hydroxyethyl)-4-methyl-3-thiazolium-chloride, 140 mL of ethanol, and 18.9 mL of triethylamine under a slightly reduced flow of argon. The reaction mixture was stirred under reflux for 3 h. It was then cooled down and poured into 1 L of ice water. The precipitate was filtered, washed with water, and dried. The product was recrystallized from ethanol. The yield was 25.51 g (51.0%). Melting point: 116 °C. Elemental analysis: Found—C: 53.42%, H: 3.55%, S: 28.35%. Calcd.—C: 53.55%, H: 3.60%, S: 28.59%.

1,2-Dithiophene-3-yl-ethan-1,2-dion

129.43 g (518.7 mmol) of $CuSO_4*5H_2O$ was diluted in 84 mL of water and 170 mL of pyridine. The solution was heated to 70 °C and 51.67 g (0.23 mole) of 2-hydroxy-1,2-dithiophene-3-yl-ethanon was added. The reaction mixture was stirred for 1 h at 80 °C. Afterwards it was cooled to room temperature and combined with 250 mL of hydrochloric acid (10%). The organic components were extracted with diethyl ether. The organic phase was dried over $MgSO_4$, filtered, and evaporated. The raw product was recrystallized from isopropanol. The yield was 41.13 g (80.32%). Melting point: 74 °C. Elemental analysis: Found—C: 54.30%, H: 2.65%, S: 28.82%. Calcd.—C: 54.03%, H: 2.72%, S: 28.85%.

Dithenyl-hydroxy-acetic Acid

41.13 g (0.185 mole) of 1,2-dithiophene-3-yl-ethan-1,2-dion was diluted in a solution of 35.06 g KOH in ethanol/water and stirred under reflux for 10 min. The reaction mixture was cooled to 0 °C and was adjusted to a pH value of 1 by adding concentrated hydrochloric acid. Afterwards the ethanol was evaporated and the reaction mixture was diluted with diethyl ether. The organic phase was extracted with saturated Na_2CO_3 solution. The Na_2CO_3 phase was decolorized with charcoal and afterwards hydrochloric acid (10%) was added to precipitate the product. The white precipitate was filtered and diluted in diethyl ether. The organic phase was dried with Mg_2SO_4 and filtered. The filtrate was evaporated. The raw product (33.11 g, 75.1% yield) was directly used in the next step without any further purification and characterization because it was unstable.

4H-Cyclopenta[2,1-b:3,4-b′]dithiophene-4-carbonic Acid

33.11 g (137.8 mmol) of dithenyl-hydroxy-acetic acid was charged into a reaction vessel which was flushed with argon. 800 mL of benzene was added. The solution was cooled to 5 °C and 57.6 g $AlCl_3$ was added. Afterwards the reaction mixture was vigorously stirred under reflux conditions for 30 min. The reaction mixture was cooled to room temperature and 30 mL of water and 200 mL of 4n hydrochloric acid were purged to the reaction mixture. The product was extracted with diethyl ether and the extract was washed with water. After drying and filtration the solvent was evaporated. The product (21.31 g, 68.9% yield) was used without any further purification. Melting point: 176 °C. Elemental analysis: Found—C: 54.23%, H: 2.55%, S: 28.97%. Calcd.—C: 54.03%, H: 2.72%, S: 28.85%.

^{1}H NMR (500 MHz, $CDCl_3$): δ [ppm]: 7.21 (dd, 4H, Ar-H, ^3J = 5.1 Hz), 4.63 (s, 1H, —CH—).

4H-Cyclopenta[2,1-b:3,4-b′]dithiophene

21.27 g (95.7 mmol) of 4H-cyclopenta[2,1-b:3,4-b′]dithiophene-4-carbonic acid and 4.3 g of Cu powder were placed into a reaction vessel, evacuated, and refilled with argon three times. Afterwards, 150 mL of freshly distilled quinoline was added and the reaction mixture was heated to reflux at about 237 °C for 40 min. It was allowed to cool down to room temperature and then it was poured into a mixture of ice and hydrochloric acid. The product was extracted with diethyl ether. The organic layer was extracted with 2n hydrochloric acid followed by saturated Na_2CO_3 solution. The organic solution was washed with water to bring it to a neutral state. The solution was dried with Na_2SO_4 and the solvent was evaporated. The raw product was further purified by column chromatography using hexane/ethyl acetate (10:1) as the eluent and by sublimation. 16.46 g of pure product was isolated (94.3% yield). Melting point: 74.5 °C. Elemental analysis: Found—C: 60.22%, H: 3.61%, S: 35.88%. Calcd.—C: 60.64%, H: 3.39%, S: 35.97%.

^{1}H NMR (500 MHz, $CDCl_3$): δ [ppm]: 7.17 (d, 2H, Ar-H, ^3J = 4.9 Hz), 7.08 (d, 2H, Ar-H), 3.53 (s, 2H, —CH₂—).

4,4-Bis(2-ethylhexyl)-4H-cyclopenta[2,1-b:3,4-b′]dithiophene

7.64 g (42.6 mmol) of 4H-cyclopenta[2,1-b:3,4-b′] dithiophene was placed into a reaction vessel, evacuated, and refilled with argon three times. 425 mL of tetrahydrofurane was injected for dilution. The solution was cooled to 0 °C, and 29.8 mL (47.8 mmol) of butyllithium solution (1.6 molar in hexane) was placed into the reaction vessel. The reaction was heated to room temperature and stirred for 2 h. It was then cooled again to 0 °C and 8.3 mL (47.8 mmol) 2-ethylhexylbromide was added. Afterwards it was stirred at 30 °C for 2 h. The same procedure with butyllithium and 2-ethylhexylbromide

addition was repeated with the same quantities and mixing times. After the second cycle, the reaction vessel was stirred overnight at room temperature. The raw material was poured out in 300 mL of saturated NaCl solution. The product was extracted twice with diethyl ether. The extracts were washed with deionized water and dried. The solvent was evaporated and the residue was purified by column chromatography with hexane as the mobile phase. Finally, 16.01 g of the pure product was isolated (93.3% yield).

Elemental analysis: Found—C: 74.37%, H: 9.69%, S: 15.79%. Calcd.—C: 74.56%, H: 9.51%, S: 15.92%.

^{1}H NMR (500 MHz, CDCl$_3$): δ [ppm]: 7.11 (d, 2H, Ar-H, ^3J = 5.0 Hz), 6.92 (m, 2H, Ar-H), 1.86 (m, 4H, —CH$_2$—), 1.10–0.80 (m, 18H), 0.75 (t, 6H, —CH$_3$), 0.59 (t, 6H, —CH$_3$).

2,6-Dibromo-4,4-bis(2-ethylhexyl)-4H-cyclopenta [2,1-b:3,4-b′]dithiophene

6.78 g (17.39 mmol) of benzyltrimethylammonium chloride and 2.61 g (24.48 mmol) of ZnCl$_2$ were added to a reaction vessel which was evacuated and refilled with argon three times. Afterwards 3.34 g (8.29 mmol) of 4,4-bis(2-ethyl-hexyl)-4H-cyclopenta[2,1-b:3,4-b′]dithiophene was diluted in 95 mL dimethylformamide and the solution was transferred to the reaction vessel. The mixture was stirred at room temperature for 90 min and then the reaction was stopped by adding 20 mL of water. The raw product was extracted with hexane. The organic phase was dried over MgSO$_4$, filtered, and evaporated. The purification was done by flush chromatography using hexane as the eluent. The yield was 4.49 g (96.3%).

Elemental analysis: Found—C: 53.47%, H: 6.69%, Br: 27.84%, S: 11.56%. Calcd.—C: 53.57%, H: 6.47%, Br: 28.51%, S: 11.44%.

^{1}H NMR (500 MHz, CDCl$_3$): δ [ppm]: 6.93 (m, 2H, Ar-H), 1.80 (m, 4H, —CH$_2$—), 1.10–0.80 (m, 18H), 0.78 (t, 6H, —CH$_3$), 0.62 (t, 6H, —CH$_3$).

2,6-Bis(4,4,5,5-tetramethyl)-[1,3,2]dioxaborolane-4,4 (2-ethylhexyl)-4H-cyclopenta[2,1-b:3,4-b′]dithiophene

4.8 g (8.56 mmol) of 2,6-dibromo-4,4-bis(2-ethylhexyl)-4H-cyclopenta[2,1-b:3,4-b′]dithiophene was placed in a reaction vessel which was evacuated and refilled with argon three times. 80 mL of tetrahydrofuran was added and the solution was cooled to −80°C. The reaction mixture was kept below −20 °C for 3 h and cooled to −80 °C again. 5.03 g (27.03 mmol) of 2-isopropoxy-4,4,5,5-tetramethyl-1,3,2-diox-aborolane was added and the reaction mixture was stirred overnight at room temperature. The reaction mixture was treated with distilled water and the raw product was extracted with diethyl ether. The organic phase was washed with water, dried, filtered, and evaporated. The purification was done by multiple flush chromatography using hexane as the eluent. The yield was 2.88 g (51.3%) of pure product. Elemental analysis: Found—C: 67.72%, H: 9.48%, S: 9.91%. Calcd.—C: 67.89%, H: 9.24%, S: 9.80%.

^{1}H NMR (500 MHz, CDCl$_3$): δ [ppm]: 7.44 (m, 2H, Ar-H), 1.86 (m, 4H, —CH$_2$—), 1.34 (m, 24H, —CH$_3$), 1.00–0.80 (m, 18H), 0.73 (t, 6H, —CH$_3$), 0.59 (t, 6H, —CH$_3$).

5,8-Dibromo-2,1,3-benzothiadiazole

25 g (0.183 mole) of 2,1,3-benzothiadiazole was placed in a reaction vessel and then 125 mL of hydrobromic acid was added. 30 mL of bromine was dropped slowly into the solution. Within 1 h after complete bromine addition, the temperature was increased to 95 °C for 4 h. The precipitate was filtered using a glass frit and washed with water to neutralize. The raw product was recrystallized from methanol/toluene (95/5).

^{1}H NMR (500 MHz, CDCl$_3$): δ [ppm]: 7.72 (2, 2H, Ar-H).

^{13}C NMR (125 MHz, CDCl$_3$): δ [ppm]: 153.0, 132.3, 113.9.

Polymerization
PCPDTBT Homopolymer

1.17 g (1.79 mmol) of 2,6-bis(4,4,5,5-tetramethyl)-[1,3,2]diox-aborolane-4,4-bis(2-ethylhexyl)-4H-cyclopenta[2,1-b:3,4-b′] di-thiophene, 0.525 g (1.79 mmol) of 5,8-dibromo-2,1,3-benzo-thiadiazole, 2.28 g (10.74 mmol) K$_3$PO$_4$, 16.16 mg (0.072 mmol) Pd(II)-acetate and 29.56 mg (0.072 mmol) of dicyclo-hexylphosphino-2′,6′-dimethoxybiphenyl were placed in a thor-oughly pre-dried reaction vessel. The reaction vessel was evac-uated and refilled three times with argon and then 40 mL of tetrahydrofurane was added. The solution was stirred for 24 h at room temperature followed by 24 h under reflux conditions. Afterwards the polymer was first end-capped using bromoben-zene followed by phenylboronic acid. The polymer was precipi-tated in methanol/2n hydrochloric acid (3:1), filtered, and dried at 40 °C. The polymer was diluted in chloroform and extracted with diluted ammonia. The organic phase was sepa-rated, washed to neutralize, precipitated, filtered, and dried. Further purification was done by soxhlet extraction using sol-vents with increasing dissolving power to separate low molecu-lar fractions. The yield was 640 mg.

Elemental analysis: Found—C: 69.20%, H: 7.19%, N: 5.34%, S: 17.35%.

^{1}H NMR (500 MHz, CDCl$_3$): δ [ppm]: 8.14 (s, 2H, Ar-H), 7.88 (s, 2H, Ar-H), 2.08 (m, 4H, α—CH$_2$—), 1.59 (m, 2H, —CH—), 1.02 (m, 16H, —CH$_2$—), 0.68 (m, 12H, —CH$_3$).

PCPDTBT-co-F8BT Polymer

0.736 g (1.125 mmol) of 2,6-bis(4,4,5,5-tetramethyl)-[1,3,2]dioxaborolane-4,4-bis(2-ethylhexyl)-4H-cyclopenta[2,1-b:3,4-b′]dithiophene, 0.209 g (0.375 mmol) of 2,7-bis(4,4,5,5-tetramethyl-[1,3,2]dioxaborolane)-9,9-dioctylfluorene, 0.441 g (1.5 mmol) of 5,8-dibromo-2,1,3-benzothiadiazole, 1.91 g (9.00 mmol) K$_3$PO$_4$, 13.15 mg (0.06 mmol) Pd(II)-acetate, and 24.6 mg (0.06 mmol) of dicyclohexylphosphino-2′,6′-dimethoxybiphenyl were placed in a thoroughly pre-dried reaction vessel. The reaction vessel was evacuated and refilled three times with argon and then 40 mL of tetrahy-drofurane was added. The solution was stirred for 24 h at room temperature followed by 24 h under reflux conditions. Afterwards the polymer was first end-capped with

bromobenzene followed by phenylboronic acid. The polymer was precipitated in methanol/2n hydrochloric acid (3:1), filtered, and dried at 40 °C. The polymer was diluted in chloroform and extracted with diluted ammonia. The organic phase was separated, washed to neutralize, precipitated, filtered, and dried. Further purification was done by soxhlet extraction using solvents with increasing dissolving power to separate low molecular fractions. The yield was 440 mg.

Elemental analysis: Found—C: 72.06%, H: 7.44%, N: 5.43%, S: 14.00%.

^{1}H NMR (500 MHz, CDCl$_3$): δ [ppm]: 8.14 (m, Ar-H), 8.02 (m, Ar-H), 7.88 (m, Ar-H), 2.08 (m, 4H, α-CH$_2$—), 1.55 (m, —CH—), 1.02 (m, —CH$_2$—), 0.68 (m, —CH$_3$).

PCPDTBT-block-F8 Polymer

Thiophene-Terminated F8-block. 2.14 g (7.78 mmol) of Ni-1,5-cyclooctadiene was placed in a thoroughly pre-dried reaction vessel. The reaction vessel was evacuated and refilled three times with argon and then 1.22 g (7.78 mmol) of 2,2′-bipyridyl dissolved in 75 mL of toluene/25 mL of dimethylformamide was added. After briefly stirring, 0.439 g (4.06 mmol) of 1,5-cyclooctadiene was added to the mixture which was stirred for 1 h at 85 °C. Afterwards a mixture of 1.86 g (3.39 mmol) of 2,7-bis(4,4,5,5-tetramethyl-[1,3,2]dioxaborolane)-9,9-dioctylfluorene and 88 mg (0.54 mmol) of 2-bromothiophene dissolved in 20 mL of toluene was added. After stirring for 4 days at 85 °C, the reaction was cooled to room temperature, dissolved in chloroform, and extracted with 2n hydrochloric acid. The organic phase was extracted with 0.1m EDTA-solution, followed by saturated NaHCO$_3$-solution. The chloroform-solution was concentrated by evaporation. The polymer was obtained by precipitation in methanol, filtration and drying in vacuum at 40 °C. The yield was 1.13 g (81.0 %).

Elemental analysis: Found—C: 79.66%, H: 9.53%, S: 2.83%.

^{1}H NMR (500 MHz, CDCl$_3$): δ [ppm]: 7.67 (m, 6H, Ar-H), 7.40 (m, Th-H), 7.30 (m, Th-H), 7.12 (m, Th-H), 2.05 (m, 4H, α-CH$_2$—), 1.12 (m 20H, —CH$_2$—), 0.80 (m, 10H, —CH$_2$—CH$_3$).

5-Bromothiophene-Terminated F8-block. 1.13 g of thiophene-terminated F8-block was placed in a reaction vessel which was filled with argon. The polymer was dissolved in 100 mL of tetrahydrofurane and the solution was cooled to 0 °C. 0.461 g (2.589 mmol) of N-bromosuccinimide was added and the reaction mixture was stirred for 3 h at 0 °C. The reaction was stopped with distilled water. Chloroform was added to extract the organic components. The organic phase was washed with water, dried, and evaporated. Further purification was achieved with column chromatography by using ethyl acetate/hexane (1:10) as the mobile phase and a short silica gel column as solid phase.

Elemental analysis: Found—C: 74.41%, H: 8.93%, S: 2.64%.

^{1}H NMR (500 MHz, CDCl$_3$): δ [ppm]: 7.67 (m, 6H, Ar-H), 7.13 (m, Th-H), 7.06 (m, Th-H), 2.05 (m, 4H, α-CH$_2$—), 1.12 (m 20H, —CH$_2$—), 0.80 (m, 10H, —CH$_2$—CH$_3$).

PCPDTBT-block-F8 Polymer. 1.025 g (1.566 mmol) of 2,6-bis(4,4,5,5-tetramethyl-[1,3,2]dioxaborolane-4,4-bis(2-ethylhexyl)-4H-cyclopenta[2,1-b:3,4-b′]dithiophene, 0.200 g (0.066 mmol) of the 5-bromothiophene-terminated F8-block, 0.441 g (1.5 mmol) of 5,8-dibromo-2,1,3-benzothiadiazole, 1.99 g (9.396 mmol) K$_3$PO$_4$, 14.09 mg (0.0626 mmol) Pd(II)-acetate, and 25.68 mg (0.0626 mmol) of dicyclohexylphosphino-2′,6′-dimethoxybiphenyl were placed in a thoroughly pre-dried reaction vessel. The reaction vessel was evacuated and refilled three times with argon followed by 42 mL of tetrahydrofurane. The solution was stirred for 24 h at room temperature and then for 24 h under reflux conditions. Afterwards the polymer was end-capped by first using bromobenzene followed by phenylboronic acid. The polymer was precipitated in methanol/2n hydrochloric acid (3:1), filtered, and dried at 40 °C. The polymer was diluted in chloroform and extracted with diluted ammonia. The organic phase was separated, washed to neutralize, precipitated, filtered, and dried. Further purification was done by soxhlet extraction using solvents with increasing dissolving power to separate low molecular fractions. The yield was 750 mg.

Elemental analysis: Found—C: 71.15%, H: 7.54%, N: 4.91%, S: 17.09%.

^{1}H NMR (500 MHz, CDCl$_3$): δ [ppm]: 8.14 (s, 2H, Ar-H), 7.88 (s, 2H, Ar-H), 2.08 (m, 4H, α-CH$_2$—), 1.55 (m, 2H, —CH—), 1.02 (m, 16H, —CH$_2$—), 0.68 (m, 12H, —CH$_3$).

F8BT Polymer. 2.249 g (3.5 mmol) of 2,7-bis(4,4,5,5-tetramethyl-[1,3,2]dioxaborolane)-9,9-dioctylfluorene and 1.029 g (3.5 mmol) of 5,8-dibromo-2,1,3-benzothiadiazole were placed in a thoroughly pre-dried reaction vessel. The reaction vessel was evacuated and refilled three times with argon and then 63 mL of tetrahydrofurane and 7 mL of toluene were added to dissolve the monomers. Afterwards 87.5 mL of a 2m Na$_2$CO$_3$ solution and 3.5 mL of a catalyst stock solution, consisting of 3.93 mg (0.0175 mmol) Pd(II)-acetate and 31.96 mg (0.105 mmol) of tris-(o-tolyl)phosphine dissolved in tetrahydrofurane/ethanol (3:1), were added. The solution was stirred for 48 h at 80 °C. Afterwards the polymer was end-capped by first using bromobenzene followed by phenylboronic acid. The polymer was precipitated in methanol/2n hydrochloric acid (3:1), filtered, and dried at 40 °C. The polymer was diluted in chloroform and extracted with diluted ammonia. The organic phase was separated, washed to neutralize, precipitated, filtered, and dried. Further purification was done by soxhlet extraction using solvents with increasing dissolving power to separate the low molecular fractions. The yield was 1.25 g (68.1%).

^{1}H NMR (500 MHz, CDCl$_3$): δ [ppm]: 8.10 (m, 2H, Ar-H), 8.03 (m, 2H, Ar-H), 7.95 (m, 4H, Ar-H), 2.15 (m, 4H, α-CH$_2$—), 1.11 (m, 20H, —CH$_2$—), 0.81 (m, 10H, —CH$_2$—CH$_3$).

OFET Fabrication

Bottom gate OFET configurations were used in conjunction with heavily doped Si-wafers as the substrates and common gate electrode. The gate dielectric was thermally grown SiO$_2$ (230 nm) with capacitance 14.6 nF/cm^2. On top of SiO$_2$,

source and drain electrodes (Au) were deposited using photolithography ($L = 10\ \mu m$, $W = 195$ mm). The wafers were cleaned with several solvents, dried under nitrogen flow, and treated with HMDS. Finally, the polymer active layers were spin-coated from chloroform solutions with concentrations of 7–10 mg/mL under inert conditions. The final film thickness was about 70 nm. Before electrical characterization, the samples were annealed in inert atmosphere. No sample encapsulation was used. The OFET characteristics were measured in dark under glove box conditions using two Source-Measure Units 236 combined with a Trigger-Control Unit 2361 and Metrics Software (all three items were from Keithley Instruments). Usually about 10 transistors were investigated for each polymer.

Cyclovoltammetry

Voltammograms were obtained on an EG and G Parc model 273 potentiostat. A three-electrode configuration was applied in an undivided cell consisting of a glassy carbon electrode (area 0.5 cm^2) in which the polymer film was deposited, a platinum mesh was used as the counter electrode and Ag/AgCl (3 M NaCl and sat. AgCl) was employed as the reference electrode.

Bu_4NBF_4 (0.1 M) in acetonitrile was used as electrolyte and prior to each measurement the electrochemical cell was deoxygenated with nitrogen. The electrochemical cell was calibrated with a ferrocene standard and the ferrocene half-wave potential was estimated to be 435 mV for this assembly. Polymer solutions (1 wt %) in CHCl$_3$ were prepared and 5 μL was deposited on the glassy carbon electrode. The prepared electrodes were kept under vacuum and dried at 60 °C for 2 h.

Photoelectron Spectroscopy

Photoelectron spectroscopy was applied for the estimation of the HOMO energy levels using a Riken Keiki AC-2. The polymers were measured as powders placed in stainless steel crucibles.

Solar Cell Fabrication and Characterization

Glass substrates coated with indium tin oxide (ITO) were obtained commercially and rinsed with isopropanol before spin coating. PEDOT:PSS (AI 4083, H.C. Stark) was spun in air and annealed at 180 °C for 15 min in N$_2$. The polymers used in this work were blended with PC$_{71}$BM in chlorobenzene with 3 vol % DIO and stirred overnight. The ratio of polymer to PC$_{71}$BM was 1:3 and the total solution concentration was 2.4 wt %. Polymer–fullerene active layers were spun at 500, 1000, or 2000 rpm in N$_2$. The cathode structure was thermally evaporated at 10^{-6} mbar and the resulting device areas were 16 or 59.5 mm^2. The solar cell structure used in this report is shown in Figure 1. Current density–voltage characteristics were measured under illumination with a light source from K.H. Steuernagel (100 mW/cm^2). The intensity of the light source was calibrated with a silicon reference diode from Fraunhofer ISE. Individual device characteristics were not corrected for spectral mismatch. Surface topographies were analyzed with an atomic force microscope (AFM) from Nanosurf in noncontact/phase contrast mode. Absorbance properties of the polymer films were measured with an ultra violet-visible (UV-Vis) spectrometer from Perkin Elmer (Lambda 950).

External Quantum Efficiency (EQE)

External quantum efficiencies were measured in the range from 300 to 950 nm. The solar cells were probed with chopped monochromatic light from a xenon short arc lamp or a halogen lamp. The resulting current was recorded using a lock-in amplifier. The photon flux incident on the sample was measured using a calibrated silicon-diode.

Photoluminescence

Photoluminescence measurements were carried out in a spectrofluorometer (Fluorolog-3, Horiba Jobin Yvon) at room temperature. The excitation wavelength was set from a double monochromator equipped with a xenon lamp. The emission from the sample was guided through a single monochromator and recorded by a photomultiplier.

CONCLUSIONS

In this work, we presented the results of the synthesis of novel donor–acceptor copolymers and their use in photovoltaic cells. PCPDTBT and F8BT (F8) were chosen as comonomer units and they were arranged in different copolymer sequences. We compared the feasibility of homopolymer mixtures, a random copolymer and a block copolymer, as the electron donor in blends with PC$_{71}$BM for solar cells. We were able to assess the impact of molecular arrangement of the monomer sequences in the copolymers on device performance. The block copolymer had a slightly higher OFET mobility than what was measured for the PCPDTBT homopolymer and for the random copolymer. From surface topography studies we infer no macroscopic differences between the phase separation modes in blends with the fullerene. This is also confirmed by PL measurements on polymer:PC$_{71}$BM films, showing fairly good exciton collection and charge transfer from the donor to the acceptor. The best photovoltaic performance of about 2%, found for the PCPDTBT-*block*-F8 polymer, is a direct result of an enhanced fill factor with respect to the other materials investigated. The results suggest a significant compatibility between the two building blocks PCPDTBT and F8BT, allowing a relatively fine tuning of the optical and electrical properties of the low band gap PCPDTBT, by selecting the copolymerization strategy and by tuning the dilution with the wide-band gap F8BT component.

REFERENCES AND NOTES

1 Brabec, C. J.; Sariciftci, N. S.; Hummelen, J. C. *Adv. Funct. Mater.* **2001,** *11*, 15–26.

2 Brabec, C. J.; Gowrisanker, S.; Halls, J. J. M.; Laird, D.; Jia, S.; Williams, S. P. *Adv. Mater.* **2010,** *22*, 3839–3856.

3 Bredas, J. L.; Norton, J. E.; Cornil, J.; Coropceanu, V. *Acc. Chem. Res.* **2009,** *42*, 1691–1699.

4 Sariciftci, N. S.; Smilowitz, L.; Heeger, A. J.; Wudl, F. *Science* **1992,** *258*, 1474–1476.

5 Ma, W.; Yang, C.; Xiong, G.; Lee, K.; Heeger, A. *Adv. Funct. Mater.* **2005,** *15*, 1617–1622.

6 Mühlbacher, D.; Scharber, M.; Morana, M.; Zhu, Z.; Waller, D.; Gaudiana, R.; Brabec, C. *Adv. Mater.* **2006,** *18*, 2884–2889.

7 Peet, J.; Kim, J.; Coates, N.; Ma, W.; Moses, D.; Heeger, A.; Bazan, G. *Nat. Mater.* **2007,** *6*, 497–500.

8 Boland, P.; Lee, K.; Gon Namkoong, G. *Sol. Energy Mater. Sol. Cells* **2010,** *94*, 915–920.

9 Chen, H.-Y.; Hou, J.; Hayden, A.; Yang, H.; Houk, K.; Yang, Y. *Adv. Mater.* **2010,** *22*, 371–375.

10 Li, W.; Qin, R.; Zhou, Y.; Andersson, M.; Li, F.; Zhang, C.; Li, B.; Liu, Z.; Bo, Z.; Zhang, F. *Polymer* **2010,** *51*, 3031–3038.

11 Soci, C.; Hwang, I.-W.; Moses, D.; Zhu, Z.; Waller, D.; Gaudiana, R.; Brabec, C.; Heeger, A. *Adv. Funct. Mater.* **2007,** *17*, 632–636.

12 Liang, Y.; Xu, Z.; Xia, J.; Tsai, S.-T.; Wu, Y.; Li, G.; Ray, C.; Yu, L. *Adv. Energy Mater.* **2010,** *22*, E135–E138.

13 Zhokhavets, U.; Erb, T.; Gobsch, G.; Alibrahim, M.; Ambacher, O. *Chem. Phys. Lett.* **2006,** *418*, 347–350.

14 Kim, C. S.; Kim, D.-Y.; Lee, S.; Kim, Y. S.; Loo, Y.-L *Org. Electron* **2009,** *10*, 1483–1488.

15 Li, G.; Shrotriya, V.; Huang, J.; Yao, Y.; Moriarty, T.; Emery, K.; Yang, Y. *Nat. Mater.* **2005,** *4*, 864–868.

16 Moet, D.; Lenes, M.; Morana, M.; Azimi, H.; Brabec, C.; Blom, P. *Appl. Phys. Lett.* **2010,** *96*, 213506–1-3.

17 Lee, J. K.; Ma, W.; Brabec, C.; Yuen, J.; Moon, J. S.; Kim, J. Y.; Lee, K.; Bazan, G.; Heeger, A. *J. Am. Chem. Soc.* **2008,** *130*, 3619–3623.

18 Moule, A.; Meerholz, K. *Adv. Mater.* **2008,** *20*, 240–245.

19 Chen, H; Hou, J; Hayden, A; Yang, H; Houk, K; Yang, Y. *Adv. Mater.* **2010,** *22*, 371–375.

20 Shin, M.; Kim, H.; Kim, Y. *Mater. Sci. Eng. B* **2010,** *176*, 382–386.

21 Chen, L.; Yang, L.; Shim, M.; Chen, H. *Sol. Energy Mater. Sol. Cells* **2010** *94*, 2244–2250.

22 McNeill, C.R.; Greenham, N.C. *Adv. Mater.* **2009,** *21*, 3840–3850.

23 Inganäs, O.; Zhang, F.; Tvingstedt, K.; Andersson, L. M.; Hellström, S.; Andersson, M. *Adv. Energy. Mater.* **2009,** *22*, E100–E116.

24 Zhu, Z.; Waller D.; Gaudiana, R.; Morana, M.; Mühlbacher, D.; Scharber, M.; Brabec, C. **2007,** *40*, 1981–1986.

25 Tsao, H.N.; Cho, D.; Wenzel Andreasen, J.; Rouhanipour, A.; Breiby, D.W.; Pisula, W.; Müllen, K., *Adv. Mater.* **2009,** *21*, 209–212.

26 Winfield, J.M.; Van Vooren, A.; Park, M.-J.; Hwang, D.-H.; Comil, J.; Kim, J.-S.; Friend, R.H. *J. Chem. Phys.* **2009,** *131*, 035104 -1–5.

27 Coffin, R.; Peet, J.; Rogers, J.; Bazan, G. *Nat. Chem.* **2009,** *1*, 657–661.

28 Di Nuzzo, D.; Aguirre, A.; Shahid, M.; Gevaerts, V.; Meskers, S.; Janssen, R. *Adv. Mater.* **2010,** *22*, 4321–4324.

29 Scharber, M.; Koppe, M.; Gao, J.; Cordella, F.; Loi, M.; Denk, P.; Morana, M.; Egelhaaf, H.-J.; Forberich, K.; Dennler, G.; Gaudiana, R.; Waller, D.; Zhu, Z.; Shi, X.; Brabec, C. *Adv. Mater.* **2010,** *22*, 367–370.

30 Jarzab, D.; Cordella, F.; Gao, J.; Scharber, M.; Egelhaaf, H.-J.; Loi, M. *Adv. Energy Mater.* **2011,** *1*, 604–609.

31 Morana, M.; Azimi, H.; Dennler, G.; Egelhaar, H.J.; Scharber, M.; Forberich, K.; Hauch, J.; Gaudiana, R.; Waller, D.; Zhu, Z.; Hingerl, K.; van Bavel, S.S.; Loos, J.; Brabec, C.J. *Adv. Funct. Mater.* **2010,** *20*, 1180–1188.

32 Teichler, A.; Eckardt, R.; Hoeppener, S.; Friebe, C.; Perelaer, J.; Senes, A.; Morana, M.; Brabec, C.; Schubert, U. *Adv. Energy Mater.* **2011,** *1*, 105–114.

33 Chen, F.C.; Tseng, H.C.; Ko, C.J. *Appl. Phys. Lett.* **2008,** *92*, 103316–1-3.

34 Li, G.; Shrotriya, V.; Huang, J.; Yao, Y.; Moriarty, T.; Emery, K.; Yang, Y. *Nat. Mater.* **2005,** *4*, 864–868.

35 Yoa, Y.; Hou, J.; Xu, Z.; Li, G.; Yang, Y. *Adv. Funct. Mater.* **2008,** *18*, 1783–1789.

36 Campoy-Quiles, M.; Ferenczi, T.; Agostinelli, T.; Etchegoin, P.G.; Kim, Y. Anthopoulos, T.D.; Stavrinou, P.N.; Bradley, D.D.C.; Nelson, J. *Nat. Mater.* **2008,** *7*, 158–164.